Supporting Information

Controlling Nitric Oxide Reduction to Ammonia on Defective α–In_2Se_3 via Ferroelectric Polarization Switching

Md Tarikal Nasir[a,b], Yun Han[a,b], Dimuthu Wijethunge[c], Aijun Du[a,b,*]

[a] School of Chemistry and Physics, Queensland University of Technology (QUT), Gardens Point Campus, 2 George Street, Brisbane, QLD 4001, Australia

[b] QUT Centre for Materials Science, Queensland University of Technology (QUT), Gardens Point Campus, 2 George Street, Brisbane, QLD 4001, Australia

[c] School of Engineering, University of Southern Queensland, 37 Sinnathamby Blvd, Springfield Central, QLD 4300, Australia

*Corresponding author: aijun.du@qut.edu.au

Computational details

Formation energy of vacancy:

The vacancy formation energy (E_f) serves as a crucial parameter for evaluating the relative stability of materials with vacancies in thermodynamic equilibrium. Typically, the formation of a vacancy is intricately linked to the synthesis environment, while the formation energy depends on the chemical potentials of the constituent elements. The thermodynamic stability of a vacancy in α–In_2Se_3 monolayer can be expressed as[1]

$$E_f = E_D - E_P + N\mu_{In} + M\mu_{Se} \quad (S1)$$

where E_D and E_P are the total energies of the defective and pristine α–In_2Se_3 monolayer. μ_{In} and μ_{Se} represent the chemical potential for single In and Se atoms, respectively, which is equal to the energy per atom in the bulk structure. *N* and *M* are the numbers of the defective In and Se atoms compared with pristine α–In_2Se_3. Herein, μ_{In} and μ_{Se} are constrained by the relationship in the α-In_2Se_3 monolayer[2]

$$\Delta H = E(In_2Se_3) - [2E(In) + 3E(Se)] = 2\mu_{In} + 3\mu_{Se} \quad (S2)$$

where ΔH is the formation enthalpy of α–In_2Se_3 and $E(In_2Se_3)$, $E(In)$, and $E(Se)$ are the total energies per unit of the α–In_2Se_3 monolayer, In bulk, and Se bulk, respectively. The energies of α–In_2Se_3, In, and Se are -19.00, -2.74, and -3.67 eV, respectively, and correspondingly ΔH is equal to -2.51 eV. The upper boundary corresponds to the Se-rich conditions, where the potential $\mu_{Se} = 0$. On the contrary, the lower boundary corresponds to the In-rich condition, where $\mu_{In} = 0$; thus, $\mu_{Se} = \Delta H/3 = -0.84\ eV$. Accordingly, we present the formation energies with respect to the chemical potential of Se ($-0.84\ eV \leq \mu_{Se} \leq 0\ eV$).

***p* band center:**

The *p*-band center (ε_p) describes the shift in the *p*-state, which is calculated as

$$\varepsilon_p = \frac{\int_{-\infty}^{0} n_p(\varepsilon)\varepsilon d\varepsilon}{\int_{-\infty}^{0} n_p(\varepsilon) d\varepsilon} \quad (S3)$$

where ε represents the electronic energy of p orbitals for the In and Se atoms, and $n_p(\varepsilon)$ is the electronic density of states in the energy level ε. The integration interval is chosen from the minimum energy to the Fermi level.

Gibbs free energy computations:

The NO reduction reaction proceeds through the transfer of a proton-electron pair ($H^+ + e^-$) to the intermediate species at each step. Hence, the change in the Gibbs free energy (ΔG) of each elementary reaction is computed by adopting the electrochemical environment-based computational hydrogen electrode (CHE) model.[3] The ΔG of each step is defined as

$$\Delta G = \Delta E + \Delta E_{\mathrm{ZPE}} - \mathrm{T}\Delta S + \Delta G_U + \Delta G_{pH} \qquad (S4)$$

where ΔE describes the difference in the computed electronic energy, ΔE_{ZPE} is the change in zero-point energy. Here, the value of temperature T is set as 298.15 K, and ΔS refers to the variation of the entropy. The vibrational frequencies of the reactive species of each elementary step during the electrochemical NO reduction reaction were computed to unravel the entropies and zero-point energies of intermediate species. The entropy and the enthalpy of the gaseous molecules were obtained from JANAF thermodynamic tables using VASPKIT.[4, 5] $\Delta G_U = -eU$, where U represents the applied electrode potential. At pH apart from 0, the free energies of reactions that H^+ takes part in are corrected by $\Delta G_{pH} = K_B T \ln 10 \times pH$, where K_B is the Boltzmann constant.[6] We calculated the key steps with applied potential of -0.5 and pH = 7 through the CP-VASP package.[7, 8]

The adsorption energies (E_{ads}) were calculated using the expression stated below[9]

$$E_{ads} = E_{Total} - E_{Slab} - E_{Adsorbate} \qquad (S5)$$

where E_{Total}, E_{Slab}, $E_{Adsorbate}$ are the energies of the adsorbed species on the catalyst, the catalyst substrate, and the isolated adsorbate, respectively.

The limiting potential (U_L) is considered to be one of the important parameters in addressing the efficiency of the catalytic material. It is defined as follows

$$U_L = -\Delta G_{max}/e \qquad (S6)$$

where, ΔG_{max} is the maximum value of Gibbs free energy change for an elementary reaction in the

NO reduction reaction process.

Additionally, to determine the energy barrier of the transition state, an improved dimer method was adopted.[10]

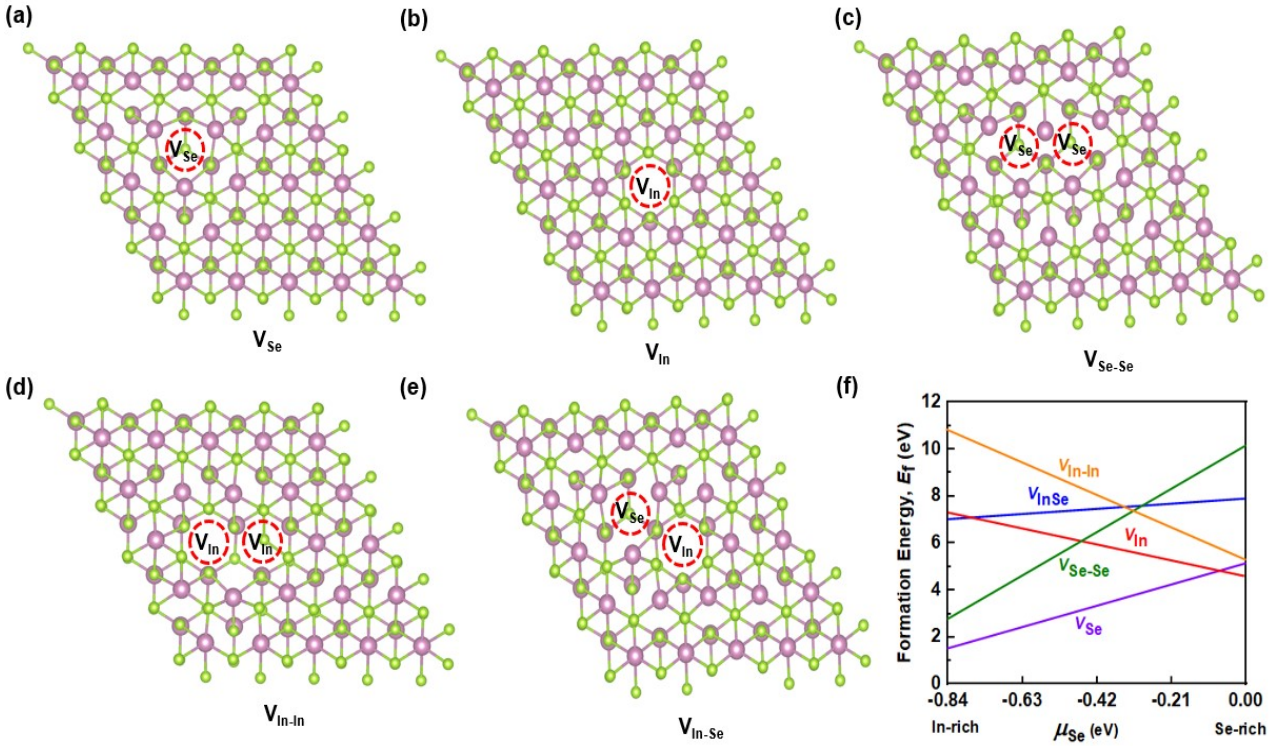

Figure S1. Top view of the optimized structures of (a) V_{Se}, (b) V_{In}, (c) V_{Se-Se}, (d) V_{In-In} and (e) V_{In-Se} for downward polarization. The purple and green balls represent In and Se atoms, respectively. (f) The evolution of formation energies of the vacancies as a function of the Se chemical potential.

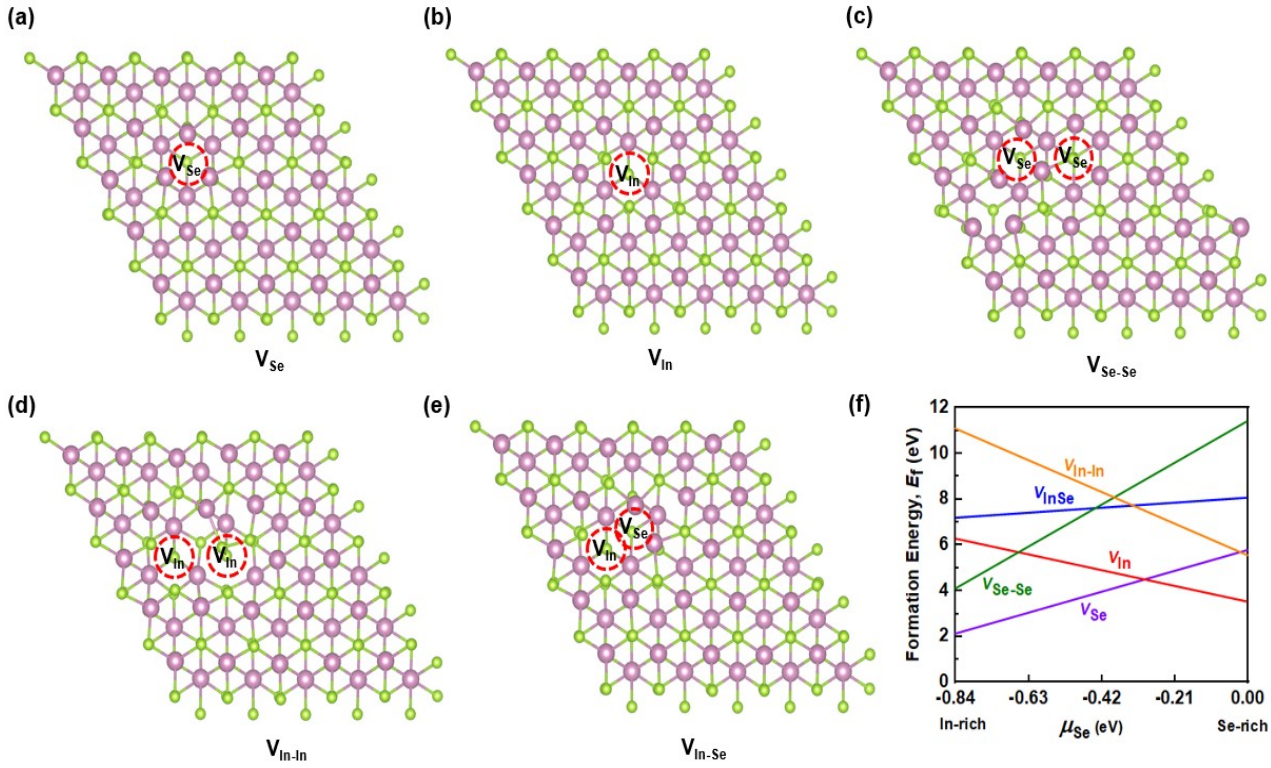

Figure S2. Top view of the optimized structures of (a) V_{Se}, (b) V_{In}, (c) V_{Se-Se}, (d) V_{In-In} and (e) V_{In-Se} for upward polarization. The purple and green balls represent In and Se atoms, respectively. (f) The evolution of formation energies of the vacancies as a function of the Se chemical potential.

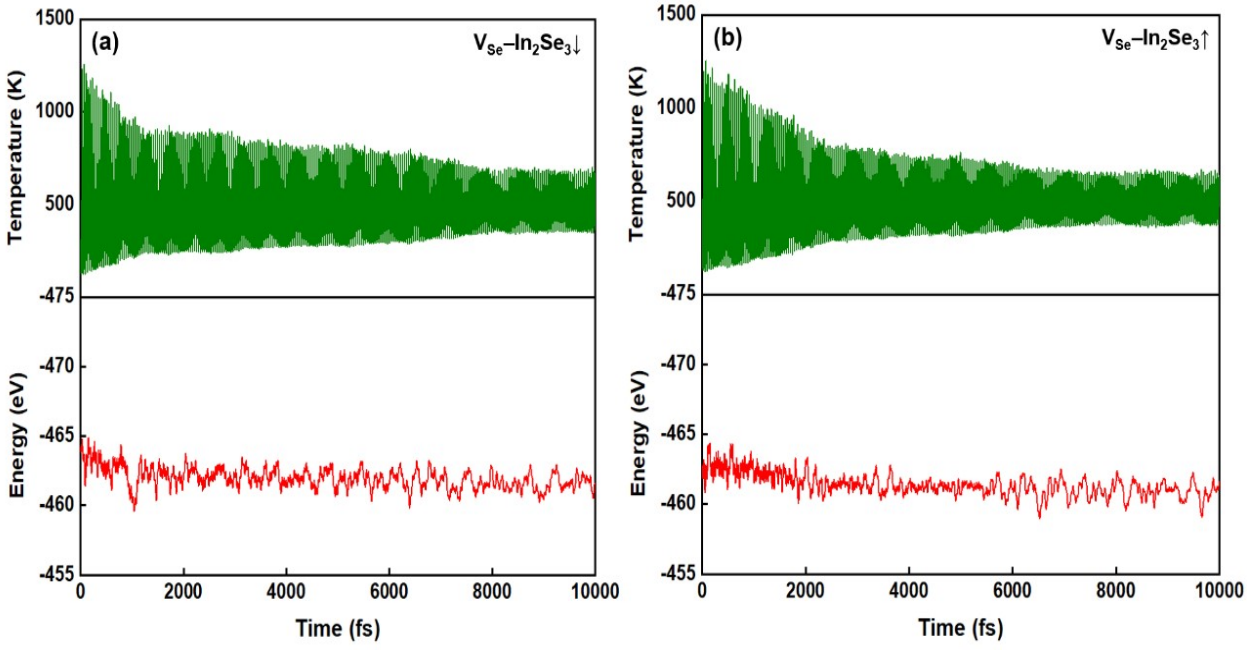

Figure S3. Fluctuations in the temperature (green line) and energy (red line) during the AIMD simulations of the (a) V_{Se}–In_2Se_3↓and (b) V_{Se}–In_2Se_3↑systems at 500 K.

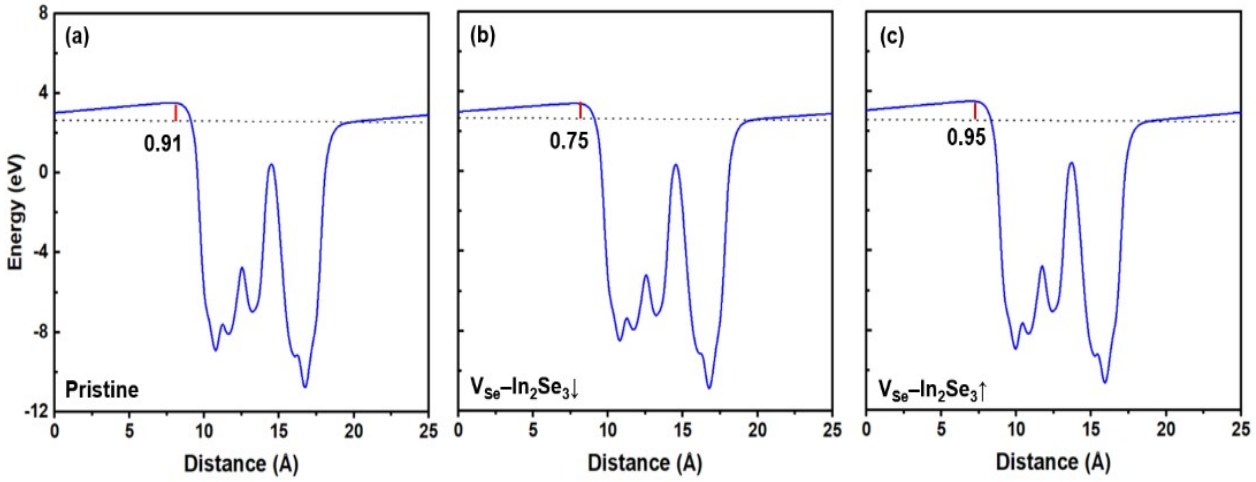

Figure S4. The average potential energy vs. distance plot for (a) Pristine α-In_2Se_3, (b) V_{Se}–In_2Se_3↓ and (c) V_{Se}–In_2Se_3↑.

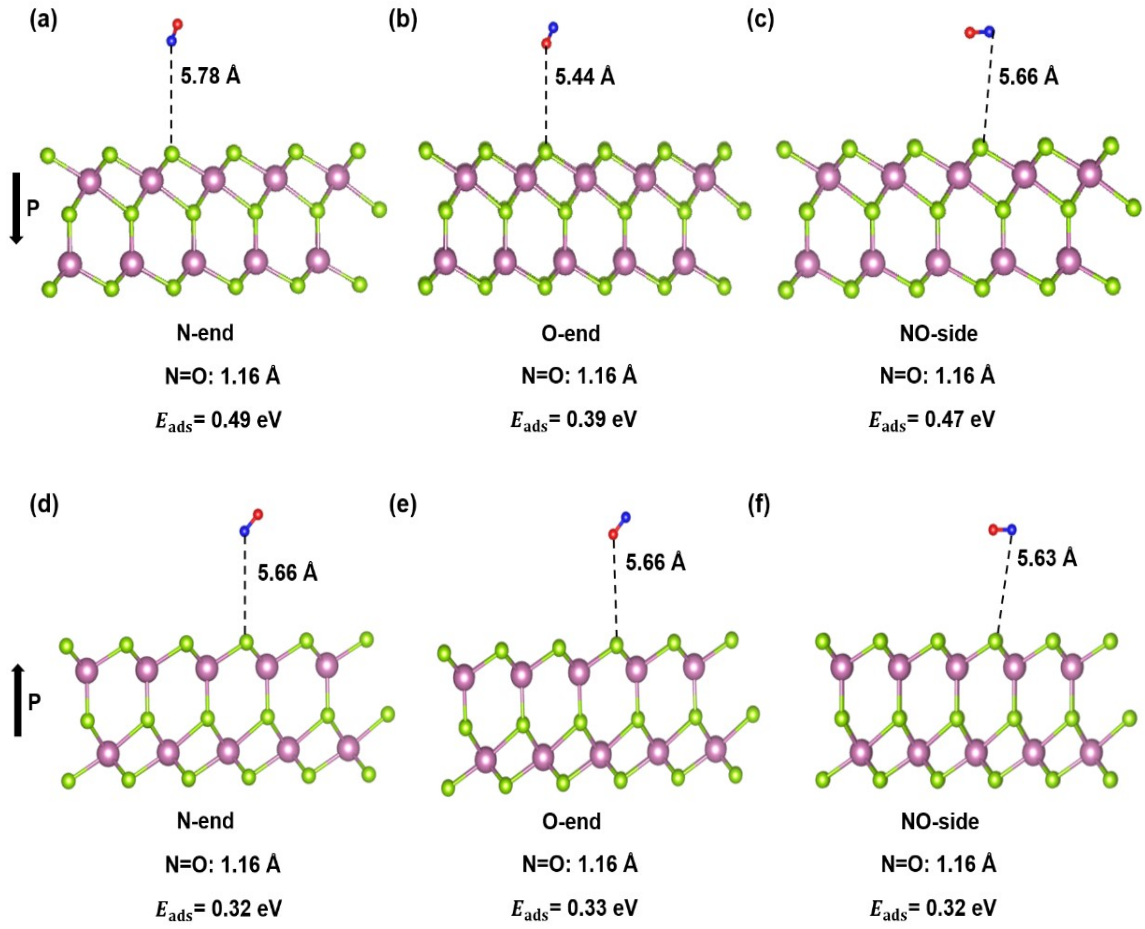

Figure S5. The side view of the (a, d) N-end, (b, e) O-end, and (c, f) NO-side adsorption on the pristine α-In_2Se_3 surface for downward (↓) and upward polarization direction (↑), respectively.

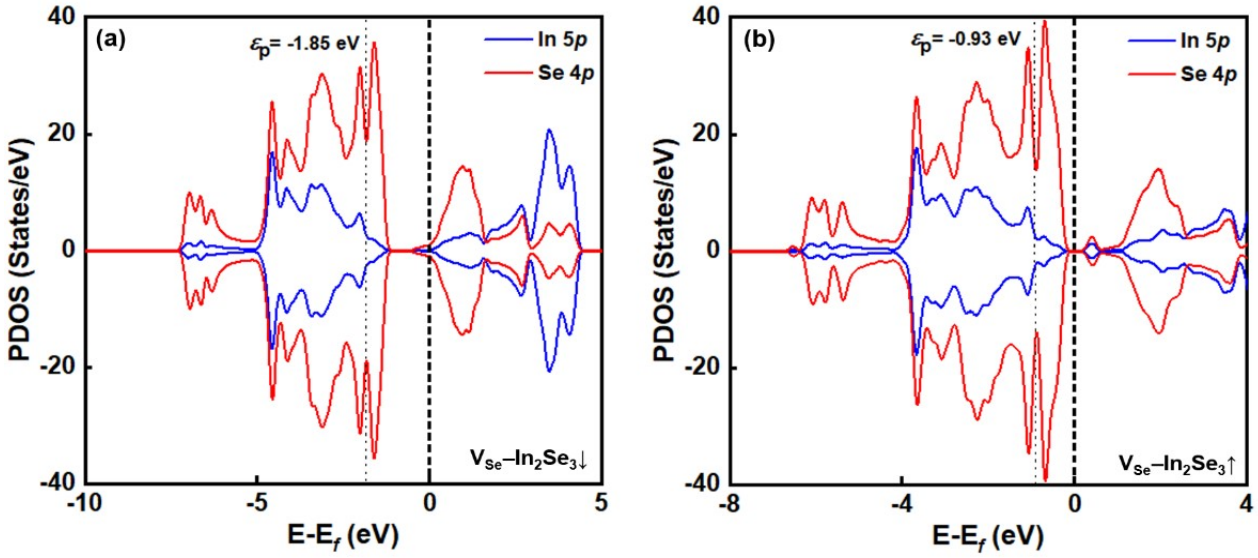

Figure S6. The calculated projected density of states (PDOS) for the *p*-orbitals of In and Se of (a) V_{Se}–In_2Se_3↓and (b) V_{Se}–In_2Se_3↑systems. The $\varepsilon_p$values denote the *p*-band center relative to the Fermi level, averaged over both spin-up and spin-down states. The switchable polarization shifts the ε_p values from -1.85 eV to -0.93 eV.

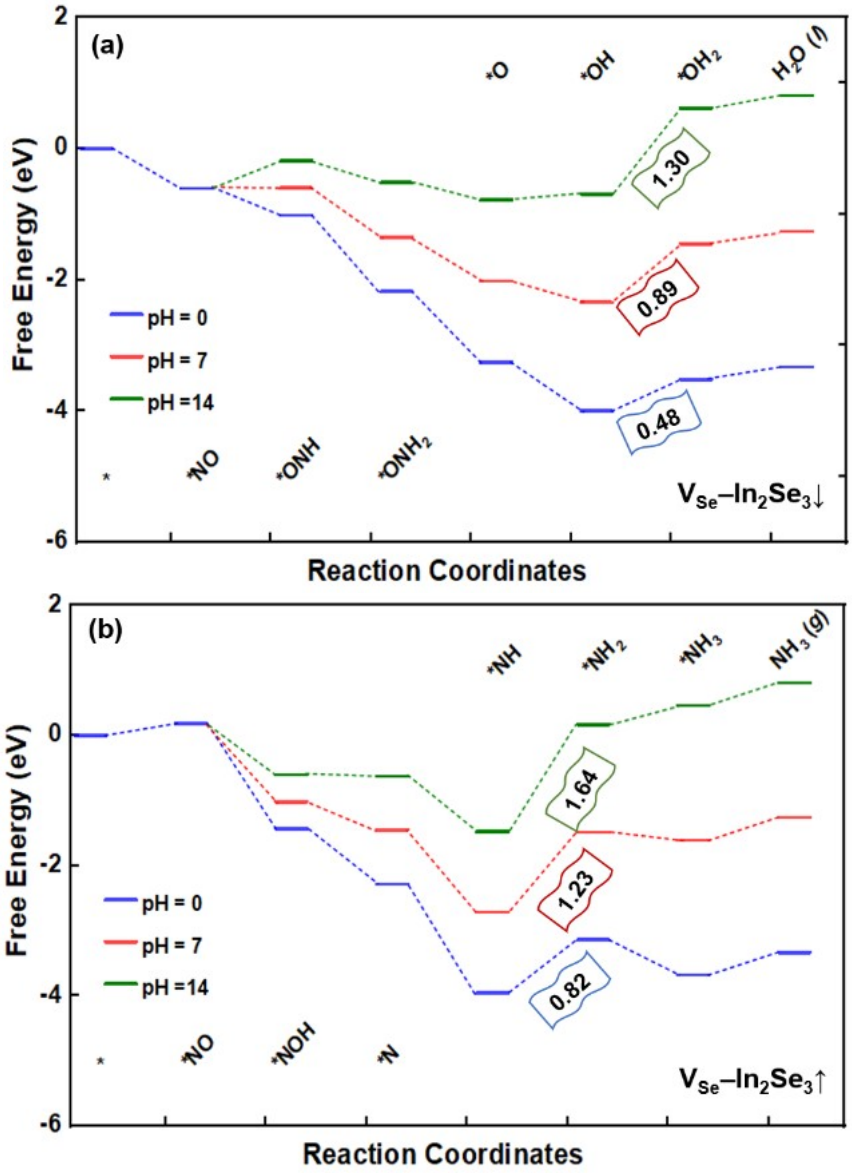

Figure S7. The free energy diagram of the electrochemical reduction of NO on (a) V_{Se}–In_2Se_3↓and (b) V_{Se}–In_2Se_3↑ with pH values of 0, 7, and 14. For V_{Se}–In_2Se_3↓at pH = 7 and pH = 14, the limiting potential increased to 0.89 and 1.30 V, respectively. In the case of V_{Se}–In_2Se_3↑it corresponds to 0.89 and 1.30 V, respectively. The increase in pH has altered the limiting potentials to higher values, but the PDS remains unchanged

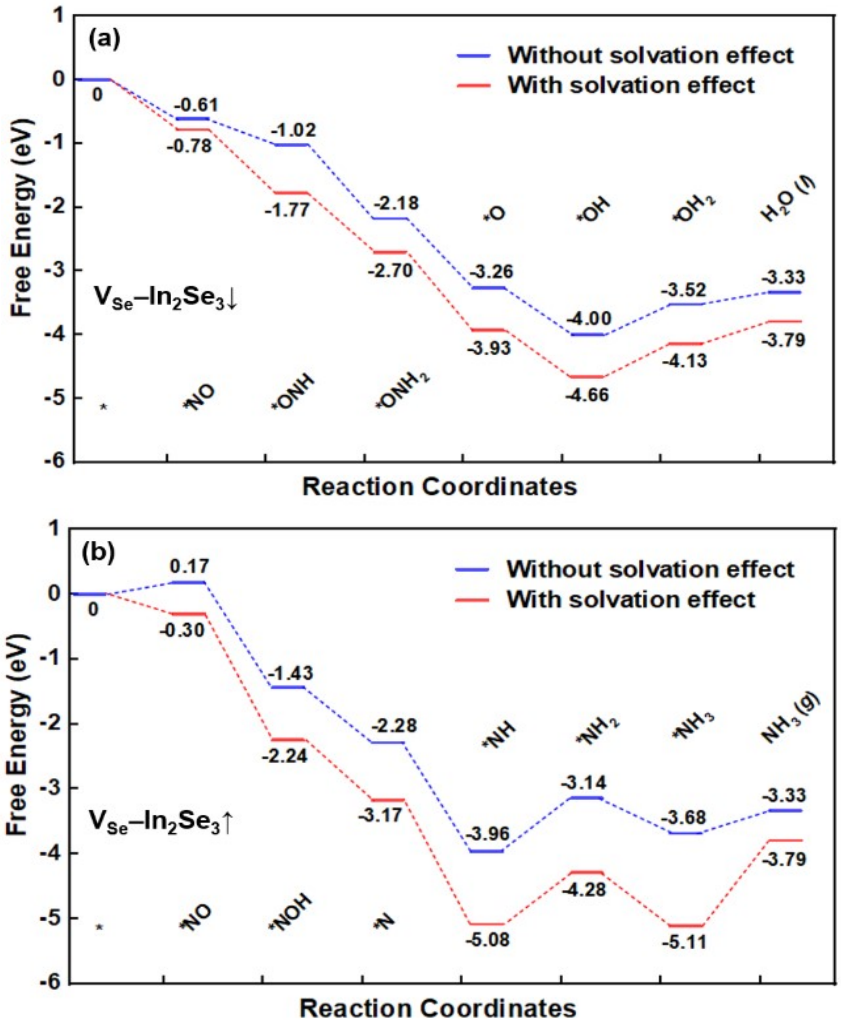

Figure S8. The free energy diagram of the electrochemical reduction of NO on (a) V_{Se}–In_2Se_3↓and (b) V_{Se}–In_2Se_3↑ systems with and without the solvation effect.

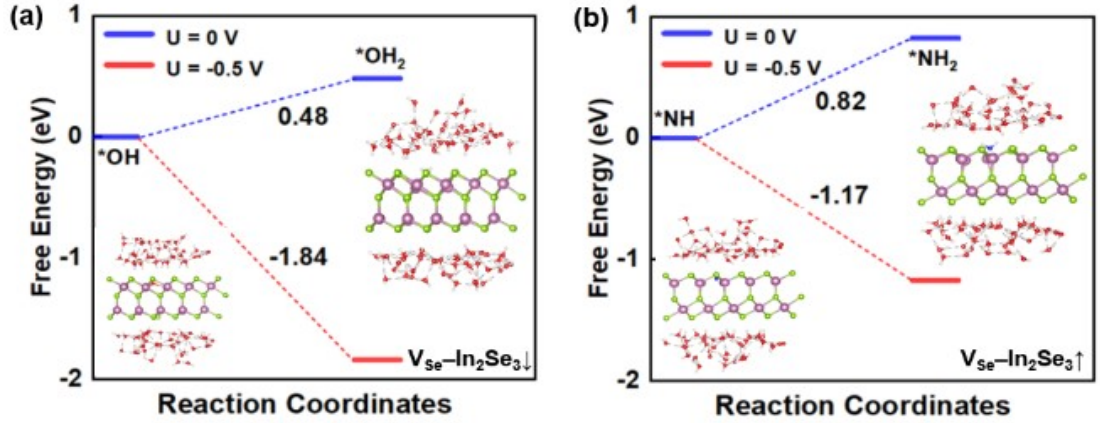

Figure S9. Comparison of the PDS for (a) V_{Se}–In_2Se_3↓ and (b) V_{Se}–In_2Se_3↑ surfaces at potentials U = 0 V and U = -0.5 V, respectively. The steps become energetically downhill under the influence of the applied electrode potential. Insets show the optimized configurations of the reaction intermediates at U = -0.5 V.

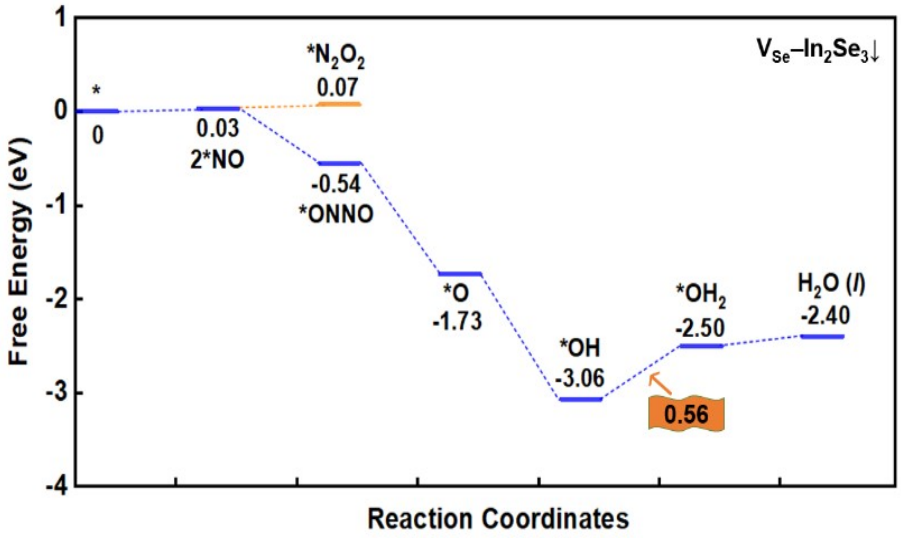

Figure S10. Free energy diagram of the NO-dimer pathway on V_{Se}–In_2Se_3↓system.

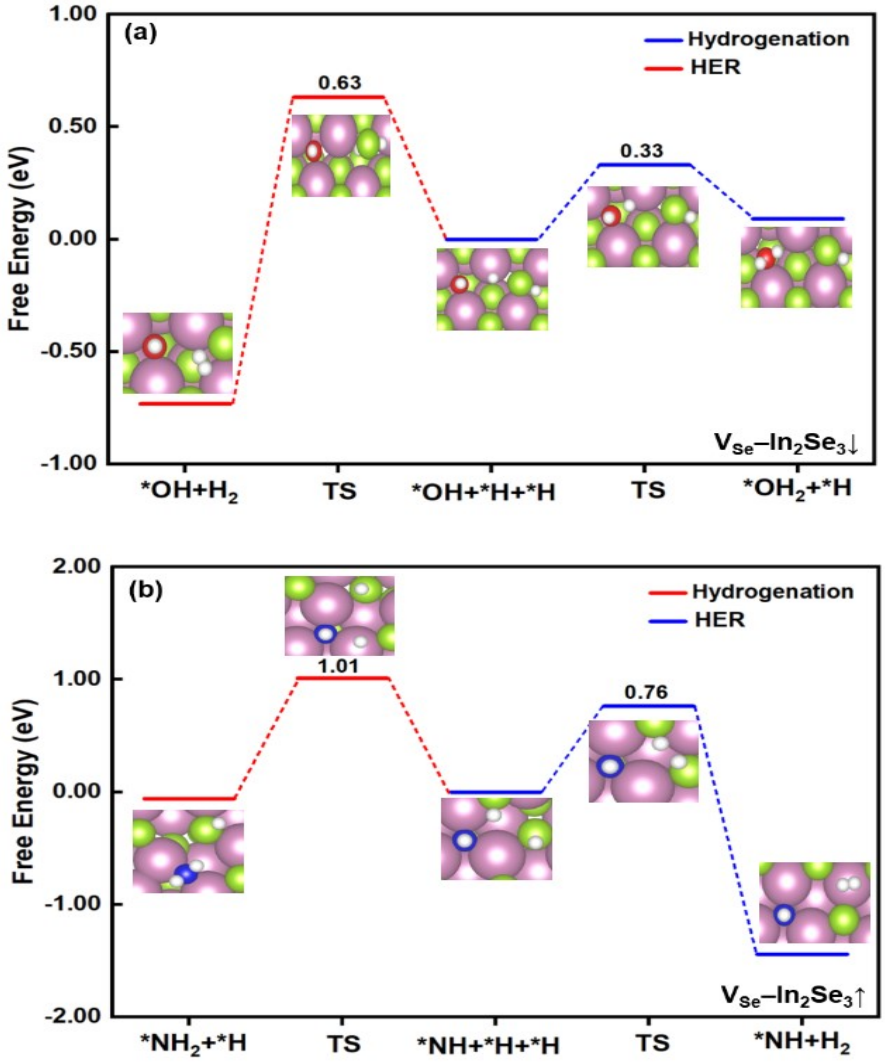

Figure S11. The comparison of the free energy barrier for the NH_3 formation and competitive hydrogen evolution on (a) V_{Se}–In_2Se_3↓ and (b) V_{Se}–In_2Se_3↑ surfaces, respectively. Insets are the optimized configurations of the intermediates.

Table S1. Out-of-plane electric polarization of the V_{Se}-In_2Se_3 monolayer.

Geometries	Polarization, P (C/m)
V_{Se}–In_2Se_3↓	15.70×10^{-10}
V_{Se}–In_2Se_3↑	6.38×10^{-10}

Table S2. Detailed numerical data for DFT calculated energy E, difference between the zero-point energy and the entropy correction ($E_{ZPE} - TS$) for adsorption species on V_{Se}–In_2Se_3↓.

Molecule/intermediates	E (eV)	$(E_{ZPE} - TS)$, eV
Slab	-469.89675	/
*NO	-483.26574	0.057946
*NOH	-487.25502	0.395351
*ONH	-487.43748	0.415769
*NHOH	-491.77305	0.740328
*ONH_2	-492.32775	0.740587
*NH_2OH	-495.40369	1.011399
*O	-477.20558	0.049355
*OH	-481.58859	0.28859
*OH_2	-484.80847	0.583879

Table S3. Detailed numerical data for DFT calculated energy E, difference between the zero-point energy and the entropy correction ($E_{ZPE} - TS$) for adsorption species on V_{Se}–In_2Se_3↑.

Molecule/intermediates	E (eV)	$(E_{ZPE} - TS)$, eV
Slab	-469.32608	/
*NO	-481.93550	0.085651
*NOH	-487.27492	0.407968
*NHO	-485.71450	0.371952
*NHOH	-490.24336	0.700322
*N	-477.05920	0.076777
*NH	-482.44350	0.380035
*NH_2	-485.31923	0.668005
*NH_3	-489.53148	0.937543

Table S4. Summary of the theoretical limiting potentials of the electrocatalytic NORR.

Catalysts	Limiting Potentials, U_L (V)	Reference
V_{Se}–In_2Se_3↓	-0.48	This work
V_{Se}–In_2Se_3↑	-0.82	This work
V_{Se}-InSe	-0.51	[11]
Cu_1@MoS_2	-0.52	[12]
Mo_2C	-0.75	[13]
Bi (012)	-0.96	[14]
Si-N_4@Gr	-0.56	[15]

References

1. R. Wang, Y. Su, G. Yang, J. Zhang and S. Zhang, *Chemistry of Materials*, 2020, **32**, 1545-1552.
2. C. Tang, L. Zhang, D. Wijethunge, K. K. Ostrikov and A. Du, *The Journal of Physical Chemistry C*, 2021, **125**, 24648-24654.
3. A. A. Peterson, F. Abild-Pedersen, F. Studt, J. Rossmeisl and J. K. Nørskov, *Energy & Environmental Science*, 2010, **3**, 1311-1315.
4. M. W. Chase, *J. of Physical and Chemical Refference Data*, 1998, 1529-1564.
5. V. Wang, N. Xu, J.-C. Liu, G. Tang and W.-T. Geng, *Computer Physics Communications*, 2021, **267**, 108033.
6. T. Hu, C. Wang, M. Wang, C. M. Li and C. Guo, *ACS Catalysis*, 2021, **11**, 14417-14427.
7. X. Zhao and Y. Liu, *Journal of the American Chemical Society*, 2021, **143**, 9423-9428.
8. S. Yu, Z. Levell, Z. Jiang, X. Zhao and Y. Liu, *Journal of the American Chemical Society*, 2023, **145**, 25352-25356.
9. N. Sathishkumar and H.-T. Chen, *The Journal of Physical Chemistry C*, 2023, **127**, 994-1005.
10. A. Heyden, A. T. Bell and F. J. Keil, *The Journal of Chemical Physics*, 2005, **123**, 224101.
11. X. Kang, Q. Fang, H. Yin, A. Du and X. Duan, *Molecular Catalysis*, 2024, **568**, 114477.
12. K. Chen, G. Zhang, X. Li, X. Zhao and K. Chu, *Nano Research*, 2023, **16**, 5857-5863.
13. K. Chen, P. Shen, N. Zhang, D. Ma and K. Chu, *Inorganic Chemistry*, 2023, **62**, 653-658.
14. Y. Lin, J. Liang, H. Li, L. Zhang, T. Mou, T. Li, L. Yue, Y. Ji, Q. Liu and Y. Luo, *Materials Today Physics*, 2022, **22**, 100611.
15. N. Saeidi, M. D. Esrafili and J. J. Sardroodi, *Applied Surface Science*, 2021, **544**, 148869.